DEVELOPMENT OF A FINITE ELEMENT METHODOLOGY FOR THE COLLAPSE ANALYSIS OF COMPOSITE AEROSPACE STRUCTURES

Adrian C. Orifici[1,2], Rodney S. Thomson[2], Richard Degenhardt[3] and Javid Bayandor[1]

[1] School of Aerospace, Mechanical and Manufacturing Engineering,
Royal Melbourne Institute of Technology
GPO Box 2476V, Melbourne, Victoria 3001, Australia
corresponding author: a.orifici@crc-acs.com.au

[2] Cooperative Research Centre for Advanced Composite Structures
506 Lorimer Street, Fishermans Bend, Victoria, 3207, Australia
r.thomson@crc-acs.com.au

[3] Institute of Composite Structures and Adaptive Systems, DLR – German Aerospace Center
Lilienthalplatz 7, 38108 Braunschweig, Germany
richard.degenhardt@dlr.de

Keywords: Stiffened structures, Postbuckling, Collapse, Interlaminar damage, Ply damage, Virtual Crack Closure Technique.

Abstract. *In this work, an analysis methodology for capturing the critical damage mechanisms leading to collapse in composite stiffened structures is proposed. One aspect of the methodology is a global-local analysis technique that monitors a strength criterion in three-dimensional local models to predict the initiation of interlaminar damage in intact structures. Another aspect of the approach was developed for representing the growth of a pre-existing interlaminar damage region such as a delamination or skin-stiffener debond. This approach is based on applying user-defined multi-point constraints in the skin-stiffener interface that are controlled based on the strain energy release rate as calculated using the Virtual Crack Closure Technique. A separate degradation model was also included to model the in-plane ply damage mechanisms of fibre fracture, matrix cracking and fibre-matrix shear. The complete analysis methodology was compared to experimental results for two fuselage-representative composite panels tested to collapse. The two panels had different geometry and material lay-ups, where one panel was tested in an undamaged state and the other had pre-damage introduced as a result of cyclic loading in the postbuckling region. For both panels, the analysis methodology was shown to be capable of accurately capturing the specimen behaviour and the way in which the various damage mechanisms contributed to the final structural collapse.*

1 INTRODUCTION

In the aerospace industry, the application of lightweight fibre-reinforced polymer materials and the use of "postbuckling" skin-stiffened structures to withstand immense loads after buckling are key technologies that have separately been used to significantly improve structural efficiency. However, to date the application of composite postbuckling structures in aircraft designs has been limited, as today's analysis tools are not capable of accurately representing the damage mechanisms that lead to structural collapse in compression. For undamaged skin-stiffened structures collapse is typically an explosive event caused by the initiation of separation between the skin and stiffener. For pre-damaged structures, such as those taken from service or those used for damage tolerance and certification studies, the pre-damaged areas can grow under compression and contribute to structural collapse. Collapse for both of these configurations is typically characterised by rapid fibre fracture, particularly in the stiffeners, which causes a significant loss of load-carrying capacity [1].

In this work, a finite element (FE) analysis methodology was developed and implemented into MSC.Marc (Marc) in order to predict the collapse of skin-stiffened structures taking degradation into account. One aspect of this methodology is a strength-based approach for analysing undamaged or intact structures that uses a global-local technique. Other aspects of the developed methodology include degradation models for capturing interlaminar damage growth and in-plane ply damage. Following a description of the developed analysis methodology, experimental results are presented for two large, blade-stiffened panels that are representative of composite fuselage designs. The panels had different skin-layups and geometry definitions, and one panel was loaded statically until collapse as an undamaged structure, whilst the other was first loaded cyclically into the postbuckling region, which generated skin-stiffener pre-damage regions prior to a static loading to collapse. Numerical models were created using the developed methodology and are shown to give very good comparison with the experimental results, with the panel behaviour, load-carrying capacity and collapse damage mechanisms accurately captured in both cases. Discussion is then given on the possible extension of the developed methodology, and its application for advanced analysis of the key damage mechanisms in composite skin-stiffened structures.

This work is part of the European Commission Project COCOMAT, an ongoing four-year project that aims to exploit the large strength reserves of composite aerospace structures through a more accurate prediction of collapse [2-3].

2 ANALYSIS METHODOLOGY

The modelling approach developed was focused on predicting the collapse of stiffened composite structures in compression by capturing the effects of the critical damage mechanisms. The approach contains several aspects: predicting the initiation of interlaminar damage in intact structures; capturing in-plane degradation such as fibre fracture and matrix cracking; and, capturing the propagation of a pre-existing interlaminar damage region [4].

The approach for predicting the initiation of interlaminar damage in the skin-stiffener interface was based on a global-local technique. In this technique, a global shell model of the full structure was used to determine the deformation field of the entire structure, which was then input as boundary conditions on a local three-dimensional (3D) brick model of a skin-stiffener interface. In the local model a strength criterion was monitored at all elements in order to predict the initiation of delamination or skin-stiffener separation. The criterion applied was the "degenerated Tsai" equation as given by Tong [5] and was defined as

$$(\sigma_x/X_T)^2 + (\sigma_z/Z_T)^2 + (\tau_{yz}/S_{yz})^2 \geq 1, \tag{1}$$

where s_x, s_z, t_{yz} and X_T, Z_T, S_{yz} are stresses and strengths in the longitudinal, through-thickness tensile and shear directions, respectively. Failure was deemed to occur when the average of all integration point values in an element satisfied this criterion. By modifying the location of the 3D local model, the initiation of interlaminar damage throughout the panel could be investigated in order to determine the most critical skin-stiffener interface location. The prediction of delamination in local skin-stiffener interfaces using this approach has been successfully demonstrated previously [6].

For the ply damage degradation model, an approach based on the Hashin [7] failure criteria and stiffness reduction method of Chang and Lessard [8] was used, as summarised in Table 1, where s_{11}, s_{22}, t_{12} and X, Y, S_{12} are stresses and strengths in the fibre, in-plane transverse and shear directions, S_{23} is the through-thickness shear strength (assumed equal to S_{12} for a transversely isotropic ply), and subscripts T and C refer to tension and compression. The criteria for fibre failure, matrix cracking and fibre-matrix shear failure were monitored and used to reduce the appropriate material properties to 10% upon detection of failure.

Failure type	Criterion	Properties reduced
Fibre, tension	$\left(s_{11}^2 / X_T^2\right)^{\frac{1}{2}} \geq 1$	E_{11}, E_{22}, n_{12}, G_{12}, G_{23}, G_{31}
Fibre, compression	$\left(s_{11}^2 / X_C^2\right)^{\frac{1}{2}} \geq 1$	
Matrix, tension	$\left(s_{22}^2 / Y_T^2 + t_{12}^2 / S_{12}^2\right)^{\frac{1}{2}} \geq 1$	E_{22}, n_{12}
Matrix, compression	$\left(\dfrac{s_{22}}{Y_C}\left(\dfrac{Y_C}{4S_{23}} - 1\right) + \dfrac{s_{22}^2}{4S_{23}^2} + \dfrac{s_{12}^2}{4S_{12}^2}\right)^{\frac{1}{2}} \geq 1$	
Fibre-matrix shear, tension	$\left(s_{12}^2 / S_{12}^2\right)^{\frac{1}{2}} \geq 1$	n_{12}, G_{12}, G_{31}
Fibre-matrix shear, compression	$\left(s_{11}^2 / X_C^2 + s_{12}^2 / S_{12}^2\right)^{\frac{1}{2}} \geq 1$	

Table 1: In-plane failure criteria and property reduction.

In the interlaminar damage growth model [9-10], pre-existing interlaminar damage in the skin-stiffener interface was represented as a debonded region between the skin and stiffener. Nominally coincident shell layers were connected with user-defined multi-point constraints (MPCs). The user-defined MPCs were given one of three "states", which were used to define the intact (state 0), crack front (state 1) and debonded (state 2) regions as shown in Figure 1. Gap elements were used in any debonded region to prevent crossover of the two sublaminates.
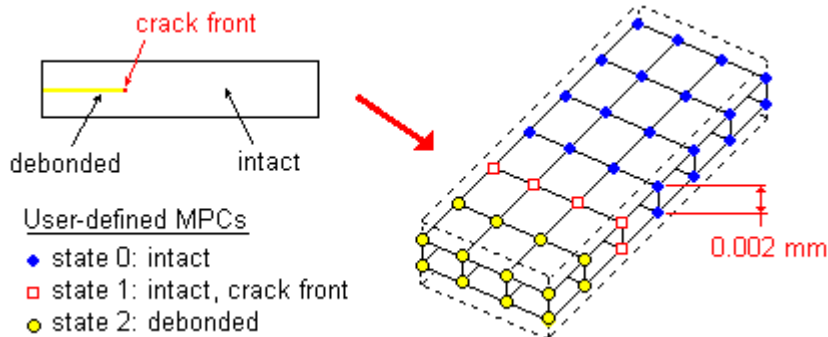

Figure 1: Interlaminar damage modelling with user-defined MPCs.

At the end of every nonlinear analysis increment, the Virtual Crack Closure Technique (VCCT) [11] was used to determine the strain energy release rates of all MPCs on the crack front. The VCCT equations accounted for arbitrary element sizes, and an algorithm was written to determine the local crack front coordinate system from the neighbouring crack front nodes, following recommendations given in Ref. [12]. The onset of propagation was determined using the B-K criterion [13], with modification for the inclusion of the mode III component following the suggestion given in Ref. [14], given by

$$\frac{\left(G_I + G_{II} + G_{III}\right)}{\left(G_{IC} + \left(G_{IIC} - G_{IC}\right)\left[\left(G_{II} + G_{III}\right)/\left(G_I + G_{II} + G_{III}\right)\right]^h\right)} = 1, \qquad (2)$$

where G are the strain energy release rates in the modes I, II and III, G_C are fracture toughness values, and h is a curve fit parameter found from mixed-mode test data. For crack propagation, an iterative method was applied, which was defined as follows:

1. At the end of every increment, the VCCT with Equation (2) was used to determine the set of crack front nodes at which crack growth or "failure" was deemed to occur.
2. The values of G_I, G_{II} and G_{III} were reduced based on the shape of local crack front to be created upon release of failing MPCs.
3. Equation (2) was used again with the reduced strain energy release rates, to determine a new set of failing MPCs.
4. Steps 2 and 3 were repeated until a consistent set of failing MPCs (or no MPCs were found to fail) using the reduced strain energy release rates.
5. Any failing crack front MPCs were then "released" or set from state 1 to state 2 for the start of the next increment.

The iterative method was an extension of the simple "fail-release" approach, which would consist of only Steps 1 and 5 as given above. The reductions in the strain energy release rate in Step 2 were necessary as it has been found that the strain energy released in propagation is dependent on the shape of the local crack front created upon crack growth. This affects the VCCT assumption that crack growth occurs in a self-similar manner, which can be violated when crack propagation is performed arbitrarily. Critically, this means that the fail-release approach, which is the method most commonly combined with VCCT to model crack propagation, can lead to significant over-estimation of the strain energy release rates, particularly in mode I crack opening. The iterative propagation method has been demonstrated in both single mode and mixed-mode investigations to give more realistic estimations of the strain energy released in crack growth than a simple fail-release approach [9-10].

The complete analysis methodology, combining the global-local analysis for interlaminar damage prediction and degradation models for interlaminar damage growth and in-plane damage, was implemented into Marc v2005r3 by a combination of user subroutines [4]. The methodology allows for a complete analysis of the postbuckling and collapse behaviour of composite structure designs, including the effects of damage. The features of the methodology make it suitable in both a design and comparative analysis context for application to both intact and pre-damaged structures. The methodology is further illustrated in Figure 2, which gives a flow chart of analysis procedures for intact and pre-damaged structures, and the interaction between intact and pre-damaged models.
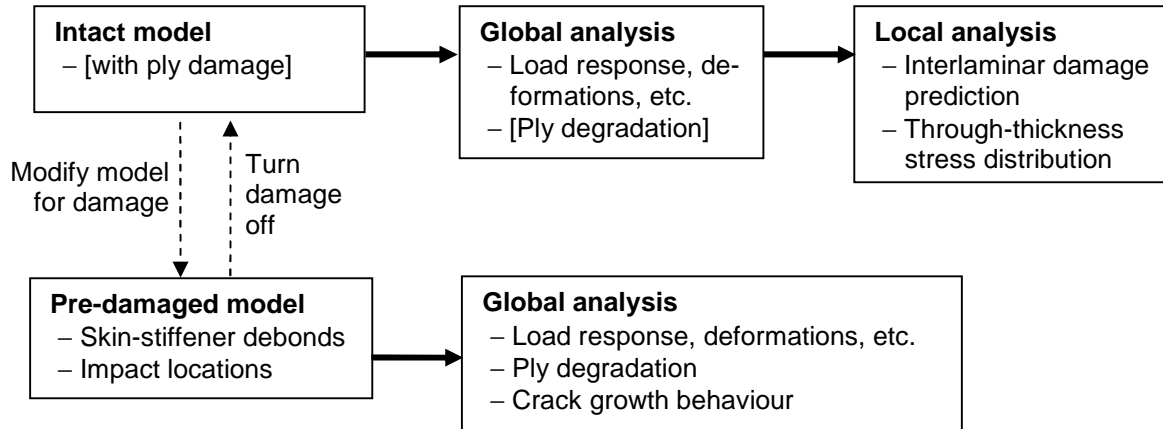
4

Figure 2: Developed methodology analysis procedure for intact and pre-damaged models

3 EXPERIMENTAL AND NUMERICAL RESULTS

In this section, results are presented for two multi-stiffener curved panels, representative of composite fuselage designs. The panels consisted of a skin and blade-shaped stiffeners, with half the stiffener lay-up on each side used to form flanges and the skin and stiffeners separately cured then bonded with adhesive. Manufacturing the flanges in this manner meant that the 45 degree flange plies were asymmetric about the stiffener blade. The two panel designs, labelled D1 and D2, used the same uni-directional (UD) pre-preg tape with different geometry and material lay-ups, as shown in Table 2 and Figure 3. The D2 panel was tested in an undamaged (intact) state whilst the D1 panel had pre-damage introduced prior to testing.

Both panels was manufactured by Aernnova Engineering Solutions and tested by the Institute of Composite Structures and Adaptive Systems of DLR (German Aerospace Center) as part of the COCOMAT project. Testing of the panels involved static loading in compression until collapse. A potting consisting of epoxy resin reinforced with sand and quartz was used at the ends of both panels to ensure an even application of the end loadings and prevent lateral movement in the testing machine. The pre-damaged panel used a longitudinal edge restraint to constrain the radial (out-of-plane) displacements along the panel side.

Parameter	D1	D2
Number of stiffeners	5	4
Total length, L	780	520
Free length, Lf	620	400
Arc length, W	560	624
Radius, R	1000	1000
Stiffener pitch, b	132	156
Skin lay-up	$[90, \pm45, 0]_S$	$[\pm45,0,90]_S$
Stiffener lay-up	$[(\pm45)_3, 0_6]_S$	$[\pm45,0_2,90_2]_S$
Ply material	IM7/8552, UD	IM7/8552, UD
Adhesive	FM 300	FM 300
Ply thickness, t	0.125	0.152
Stiffener height, h	14	28.9
Stiffener width, w	32	56

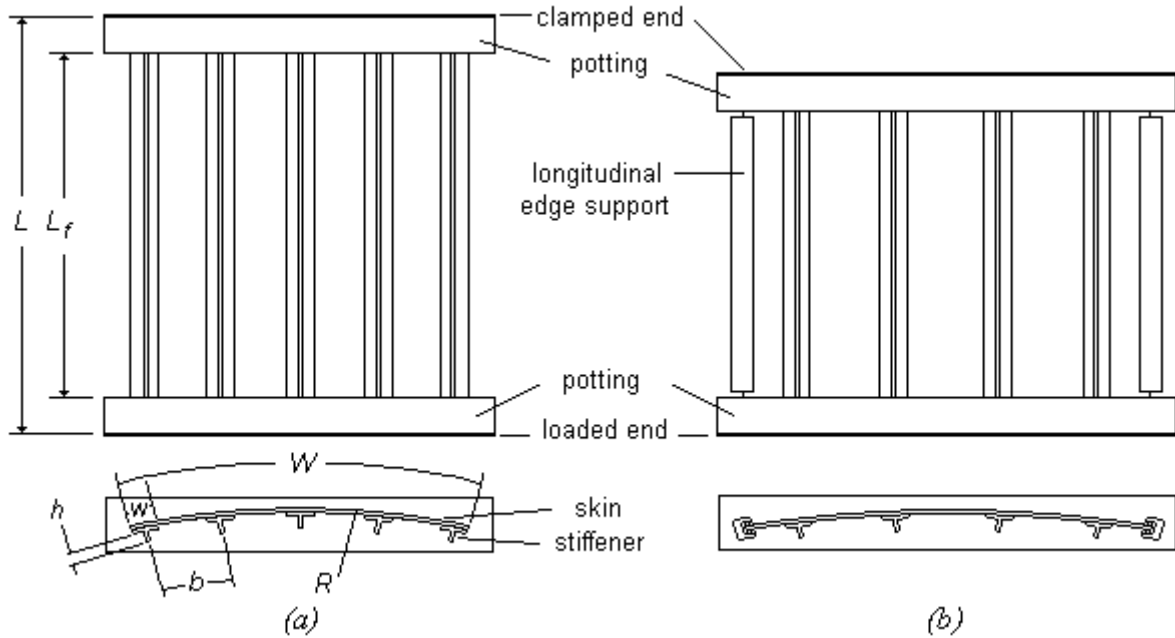Table 2: Nominal D1 and D2 panel details, all dimensions in mm.

Figure 3: Panel geometry (a) D1 (b) D2.

Following manufacture, panel quality was inspected with ultrasonic and thermographic scanning and panel imperfection data was measured using the 3D optical measurement system ATOS. During the test, measurements were taken using displacement transducers (LVDTs), strain gauges, the 3D optical measuring system ARAMIS, and optical lock-in thermography. Piezoelectric patches were also used to input and measure mechanical waves in the panels throughout testing, though the data from these devices is not presented in this paper. Further detail on all the inspection and data measurement systems can be found in Ref. [15].

3.1 Intact panel (D2)

The D2 panel was manufactured and inspected according to the specimen details and inspection procedure outlined previously. The ultrasonic and thermographic scans found no damage in the panel after manufacture. Under compression, the panel developed a range of buckling mode shapes, as shown in Figure 4. Global buckling occurred at 0.47 mm axial compression and corresponded to one buckle in the outer stiffener bays. The buckles were not symmetric, and appeared to be influenced by the imperfection pattern, which showed a region of initial displacement towards the centre of curvature at a panel corner. One of the global buckles was offset from the panel centreline towards this corner, and the bay with this offset buckle developed a second buckle at 0.57 mm axial compression. Under further compression the panel displayed a range of complex mode shape changes, which included a global buckle in the centre stiffener bay at 0.65 mm, and a second buckle in the other outer stiffener bay at 1.37 mm. During the test, thermographic scans were taken at load levels before and after buckling, and following collapse, though no damage was seen in the panel prior to collapse. Panel collapse occurred at 1.84 mm axial compression, or 174 kN applied load, and was characterised by fibre fracture in the stiffener and delaminations under all four stiffeners.
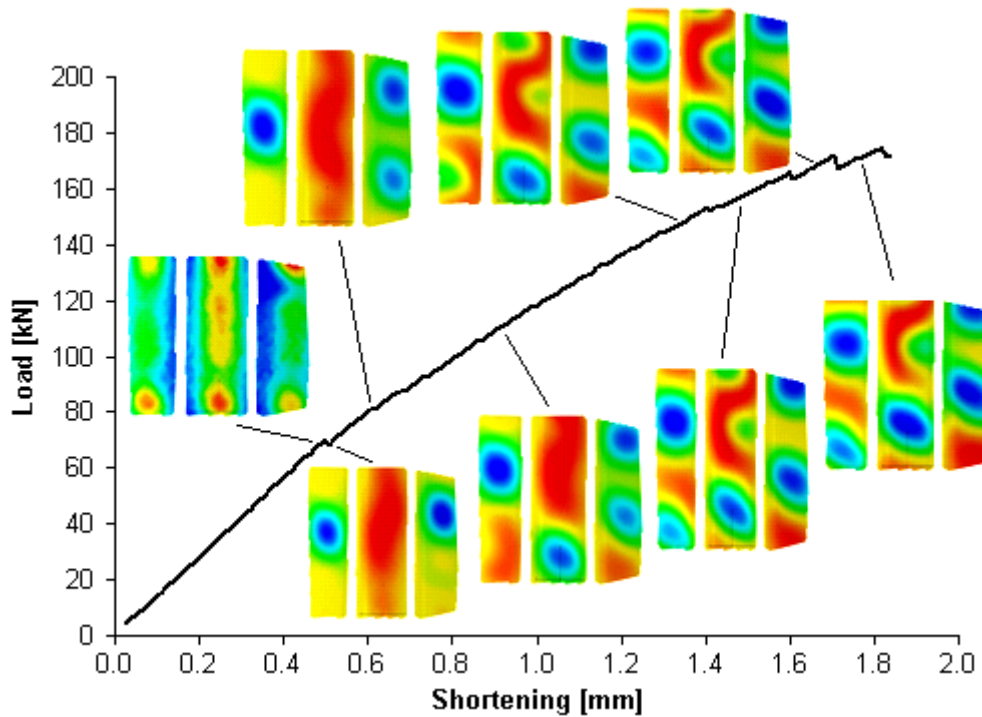
Figure 4: D2 experimental load-shortening, with radial displacement contours (stiffener side).

For the numerical analysis, the global-local analysis technique described previously was applied in order to predict the collapse of the structure by capturing the critical damage mechanisms of fibre fracture and skin-stiffened separation. The global FE model consisted of 6,413 nodes and 6,032 shell elements, with boundary conditions as shown in Figure 5. The local model used a ply-level mesh refinement with eight elements in the longitudinal direction, and consisted of 34,376 nodes and 27,736 solid brick elements. The local model with the strength criterion for interlaminar damage was applied at a number of locations throughout the panel, in order to determine the most critical skin-stiffener interface location.

Figure 5: D2 FE model with boundary condition (BC) definition.

The models were analysed in Marc v2005r3 using the nonlinear solver with a full Newton-Raphson procedure and a load residuals tolerance of 0.01. The load-displacement and failure predictions are given in Figure 6 and Figure 7, where debond initiation was predicted to occur at 1.92 mm axial compression, which preceded the onset of collapse at 2.08 mm compression. The FE model showed buckling of five to six half sine waves per stiffener bay from about 0.65 mm axial compression, where under further compression one or two half waves became dominant and showed larger deformation. There was continual change of the buckling shape until around 1.22 mm compression, at which point a stable and symmetric buckling pattern developed of three half waves per bay, as shown in Figure 7(a), and this continued until the onset of fibre fracture in the stiffeners causing collapse. From the local model investigation, the critical skin-stiffener interface was at the panel centre, with interlaminar damage predicted at the stiffener flange edge in the centre stiffener bay.
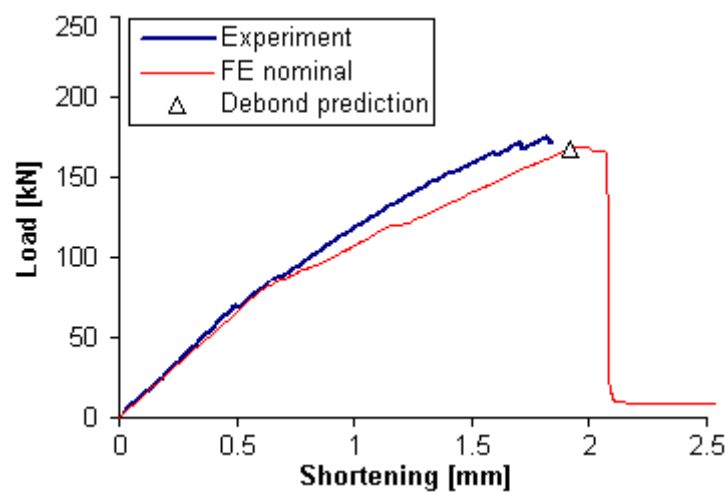

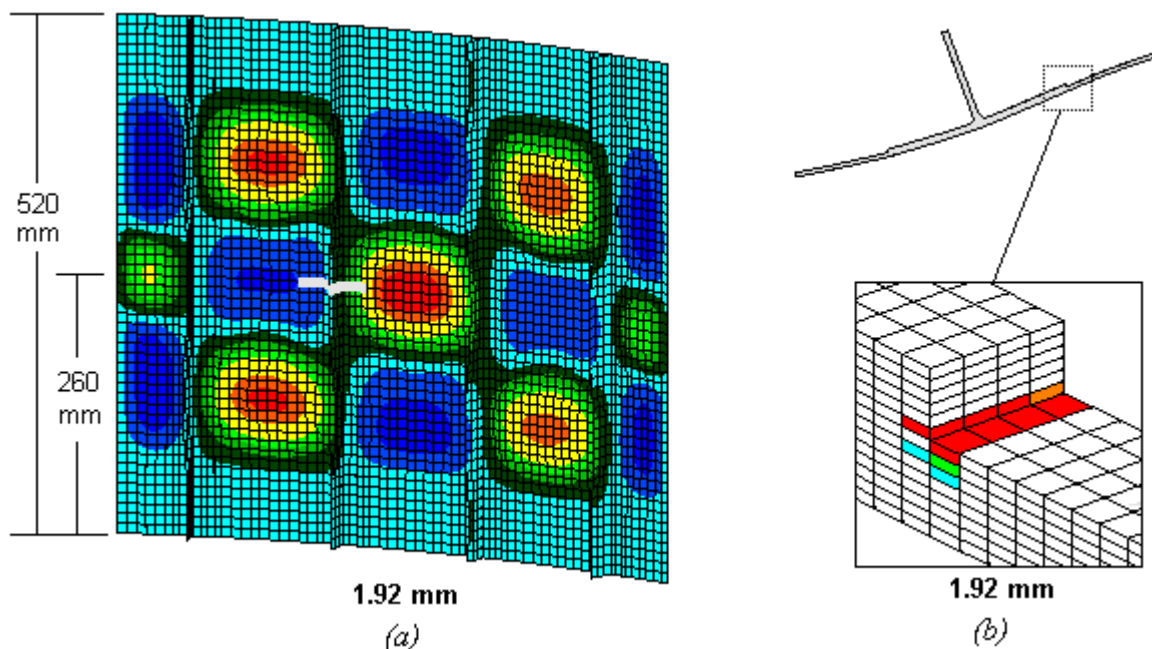Figure 6: D2 panel, load-shortening and debond prediction, experiment and FE models.

Figure 7: D2 panel, (a) global model with local location shown (b) local model.

8

In comparison with experiment, the global FE model was not able to predict the exact asymmetric buckling patterns seen experimentally, and the predicted structural stiffness was lower than the experimental value, particularly in the postbuckling region. In spite of this, the panel behaviour and onset of buckling were predicted well. The predicted initiation of debonding also compared very well with the experimental collapse of the panel, though the exact location of failure was not predicted as this was dependent on the deformation. However, investigation of local models at other locations revealed that the interlaminar damage was predicted to occur at multiple locations throughout the panel within a small range of compression values up to the point at which fibre fracture occurred. These locations included anti-nodal and nodal lines, where the anti-nodal lines such as that shown in Figure 7 gave failure at the flange edge due to high peel stresses, and the nodal lines of minimum displacement failed in the region underneath the stiffener due to high shear stresses.

3.2   Pre-damaged panel (D1)

The D1 panel was manufactured and inspected as previously described, with no damage found from the ultrasonic and thermographic scanning following manufacture. In testing, the panel was loaded with 2000 cycles up to 1.08 mm compression, 1700 cycles up to 1.93 mm compression, then statically until collapse. The cyclic loading corresponded to loads just before global buckling, and 95% of the expected displacement at collapse. Following an assessment of the results, it was seen that the cyclic loading, particularly the 95% loading, caused damage to occur in the panel that was considered as pre-damage for the final static loading to collapse. The experimental results are presented below, where Figure 8 is the load-displacement curve with out-of-plane displacement fringes and Figure 9 shows thermographic and ultrasonic scans of the panel damage before and after the final static loading.

Under loading the panel developed a local buckling pattern at around 0.75 mm axial compression of 13 to 15 longitudinal half waves per stiffener bay, leading to global buckling at around 1.0 mm axial compression. The global buckling pattern was symmetric and consisted of an inwards buckle (towards the stiffener side) located over the centre stiffener and outwards buckles in the outer stiffener bays. Under further compression the central buckle moved to one of the inner stiffener bays creating an asymmetric pattern.

In cyclic loading, periodic thermographic scans were used to monitor damage, and no damage was seen in the panel after the first 2000 cycles. After 400 cycles at the higher cyclic load, skin-stiffener debonding became evident at two locations in the centre and an inner stiffener. These areas were seen to grow under further cyclic loading, so that at 3700 cycles, when the cyclic loading was completed, the damage was as shown in Figure 9(a).

Under static loading the same local and global buckling patterns seen in cyclic loading developed, though some opening of the debonded regions was evident by 2.5 mm axial compression. At around 2.5 mm axial compression the debonded areas showed a rapidly increased damage growth and opening displacement, which caused a large reduction in the load-carrying capacity of the panel, as seen in Figure 8. The damage growth process was seen again at around 2.81 mm axial compression, where growth of the debonded area led to an increase in the skin-stiffener opening, and also caused some fibre fracture and matrix cracking in the regions around the debonds. Collapse of the panel occurred at 3.31 mm axial compression and corresponded to significant fibre fracture through the centre stiffener.
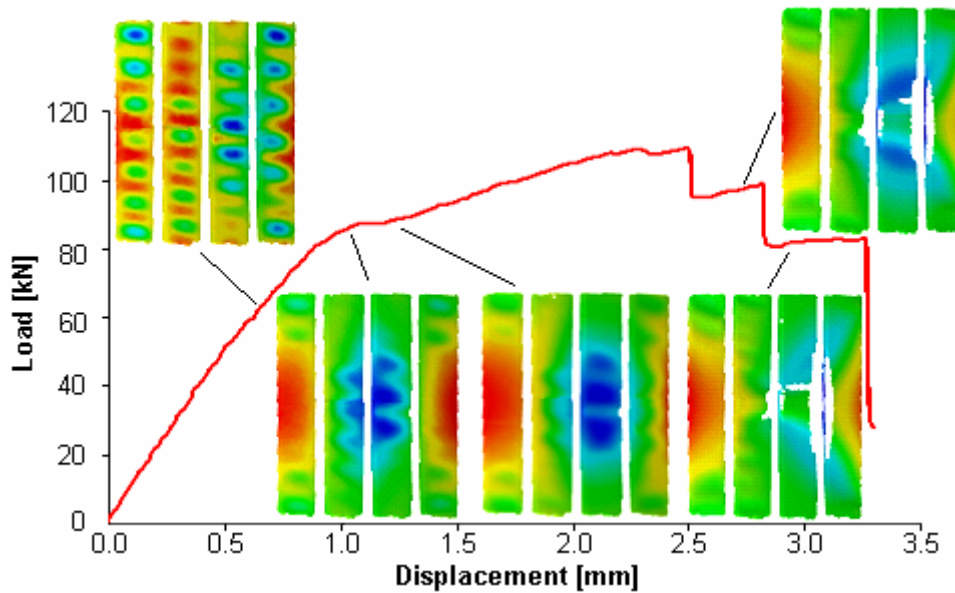
Figure 8: D1 experimental load-shortening, with radial displacement contours (stiffener side) [15].
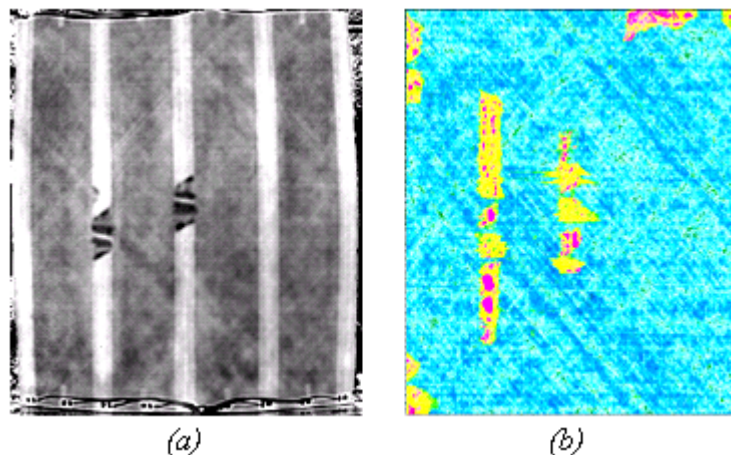

Figure 9: D1 panel (a) thermography scan after 3700 cycles (b) ultrasonic scan after collapse (skin side) [15].

In the numerical analysis, an FE model was created based on the analysis methodology described, and consisted of 6,004 nodes and 5,772 shell elements. The boundary conditions were similar to those shown for the D2 panel in Figure 5, though the longitudinal restraint was removed. User-defined MPCs were included between the skin and stiffener of the centre and an inner stiffener, in order to model the debond growth seen in the experiment. Skin-stiffener debonds were created as pre-damage by setting the MPCs to the appropriate states. The pre-damaged debonded regions were taken from the thermographic scans of the damage, seen in Figure 9(a), and were adapted to the regular grid mesh of the model to most closely match the area and shape of the experimental damage sites. It was assumed that the cyclic loading only resulted in skin-stiffener debonding, and any other damage such as matrix cracking that could have been present in the panel prior to static loading was not considered.

The model was analysed in Marc v2005r3 using the nonlinear solver with a full Newton-Raphson procedure and a load residuals tolerance of 0.01. The results are given below, where Figure 10 is the load-displacement behaviour, Figure 11 gives the out-of-plane deformation and Figure 12 illustrates the debond growth.
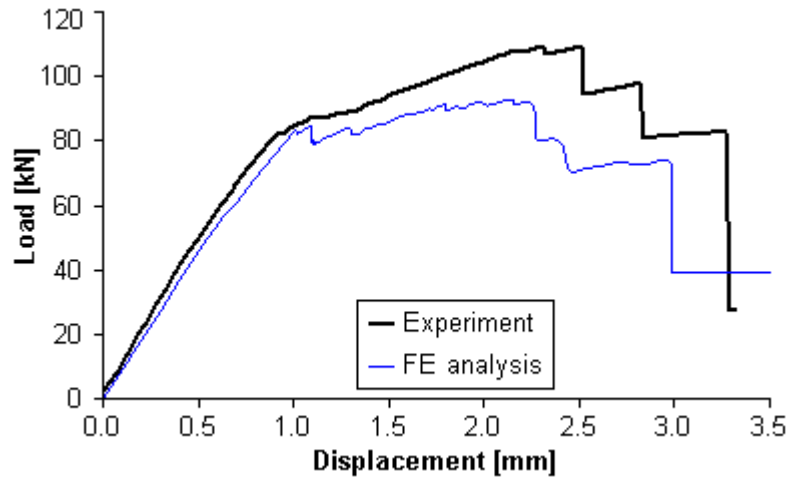
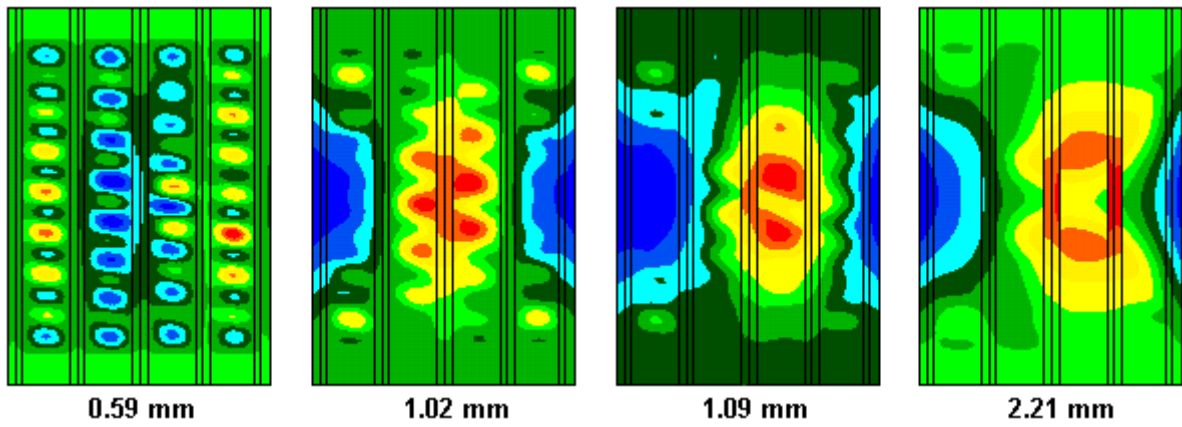Figure 10: D1 panel, load-displacement curve, experiment and FE model

| 0.59 mm | 1.02 mm | 1.09 mm | 2.21 mm |

Figure 11: D1 panel, out-of-plane deformation (stiffener side).
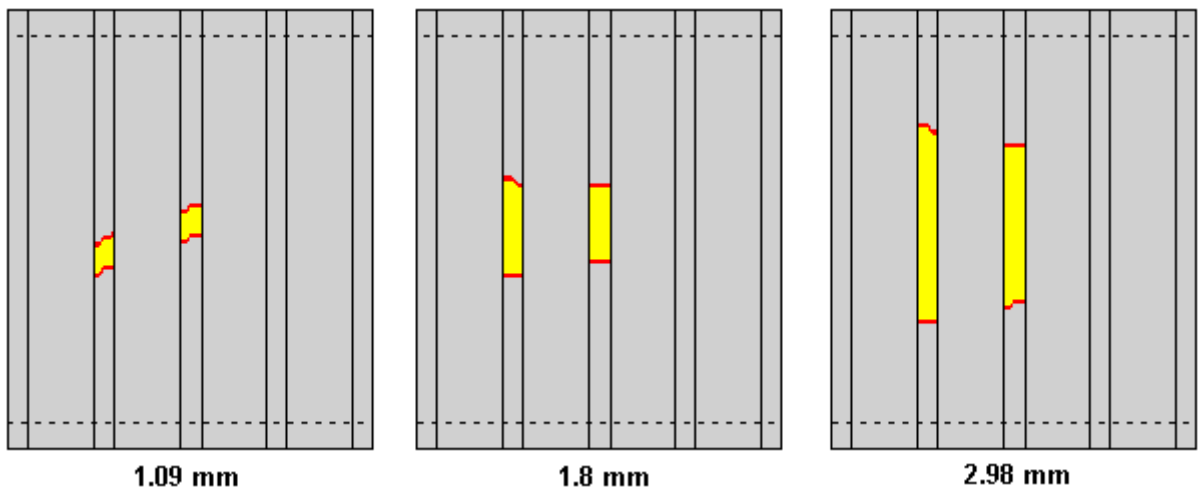

| 1.09 mm | 1.8 mm | 2.98 mm |

Figure 12: D1 panel, debonded area at applied displacement (skin side).

11

From Figure 11, the FE model gave a local buckling pattern of 15 half waves per bay, global buckling of a single central buckle at 1.02 mm compression that moved to be located between two inner stiffeners by 1.09 mm compression, all of which agreed very well with the experimental behaviour shown in Figure 8. In the numerical model, the movement of the global buckle coincided with coalescence of the separate debonded regions under the two stiffeners, and some opening was seen across these interfaces. Growth of the debonded regions was then predicted to occur in a continuous manner, and was characterised by drops in the load response and increased skin-stiffener opening. This was accompanied by matrix cracking in mainly the outer 90° plies of the skin, which was focused on the centre and edges of the debonded regions. Though correspondence was not seen at all predicted locations, the experimental panel did show matrix cracking in the outer plies extending from the skin-stiffener debond edges.

Under further compression, the numerical model showed fibre fracture in mainly the central 0° stiffener plies at 2.25 mm, 2.35 mm and 2.96 mm axial compression, with the two outer stiffeners and an inner stiffener failing sequentially. Fibre fracture was characterised by large drops in the load response of the panel of around 10 kN for the outer stiffener failures, and around 30 kN for the inner stiffener, where the latter was taken as the collapse of the panel. Though the experimental panel showed failure in the central stiffener causing collapse, the sequence and size of the load reductions, the onset of fibre fracture in the central 0° plies of the stiffeners, and the way in which the debond growth and matrix cracking contributed to fibre fracture and panel collapse all closely matched the experimental results.

Whilst it was difficult to extract precise crack growth data from the experimental results, crack opening was seen at several stages before and after fibre fracture, and the experimental debonded area under the inner stiffener showed the greater crack growth, both of which compared well with the numerical model. Additionally, the approximate final debonded lengths of the experimental panel were 224 mm and 403 mm under the central and inner stiffener respectively, which gave very good comparison with the numerical values of 282 mm and 316 mm, especially considering the fact that fibre fracture in the experimental panel would have caused additional crack growth and energy released.

4   DISCUSSION

For all analyses, there were a number of factors that considerably influenced comparison with experimental results. One aspect was the difficulty in accurately capturing the correct buckling mode shapes and deformation patterns, which was especially critical for crack growth in the region just ahead of any crack front. Also, the influence of mesh density remains significant for any analysis, where though the effect on strength-based failure predictions was uncertain, using smaller elements would have led to reduced strain energy release rates and less conservative predictions in all crack growth analyses. Separately, for the comparison with the cyclically-loaded experimental panel, the effect of the repeated loading into deep postbuckling on the integrity of the panel and general structural behaviour remains largely uncertain. In spite of these aspects, the developed approach allowed for in-depth analysis of the critical damage mechanisms, and was able to illustrate the way in which these mechanisms combined to produce final panel collapse.

One aspect that remains important in the application of the developed approach for both design and analysis is the computation time. For the analysis presented, computation times were dependent on the extent of crack growth and fibre fracture, and range from 40 minutes to more than a week for models where these factors were significant. In general, this order of computation time fits in with the aims of the developed approach to form part of a necessarily "slow" analysis tool suitable for aircraft certification. However, a more efficient process

would obviously be desirable, and can be achieved in a number of ways, including increasing the efficiency of the subroutine code, using a less severe knockdown of properties in ply softening, and applying the degradation models to selected regions only. However, it must remembered that the accurate analysis of crack growth and ply failure is always going to be computationally expensive, and that experience is required apply the degradation models within practical design and analysis procedures.

Overall, results presented demonstrated the capability of the developed approach to provide accurate predictions of the behaviour of postbuckling composite stiffened panels, and critically to capture the damage mechanisms for compression loading. The methodology has application for the design and analysis of the next generation of aircraft structures, as it allows for the large potential for efficiency gains from using postbuckling design to be used with composite materials.

5 CONCLUSIONS

In this work, an analysis methodology for capturing the critical damage mechanisms leading to collapse in composite stiffened structures was proposed. One aspect of the methodology was a global-local analysis technique that monitored a strength criterion in cross-section models to predict the initiation of interlaminar damage in intact structures. A degradation model was developed for capturing in-plane ply damage due to fibre fracture, matrix cracking and fibre-matrix shear that was based on the criteria of Hashin [7] and property reduction method of Chang and Lessard [8]. A separate degradation model was developed for representing crack growth in the skin-stiffener interface in which user-defined MPCs are controlled using the VCCT. All approaches were implemented into the nonlinear analysis solver of Marc v2005r3 using a combination of user subroutines.

Experimental results were presented for fuselage-representative composite panels loaded in compression to collapse, in both intact and pre-damaged configurations. For the intact panel, failure occurred in the postbuckling region due to the onset of skin-stiffener debonds and delaminations, which led to catastrophic collapse. For the pre-damaged panel, skin-stiffener debond regions were created by first loading the panel cyclically into the postbuckling region. Upon final static compression to collapse, the skin-stiffener pre-damage regions grew, and led to sequential failure in the panel stiffeners. For both intact and pre-damaged panels, the analysis methodology was able to successfully capture the specimen behaviour and critical damage mechanisms, and gave realistic predictions of the panel collapse. The application of the methodology in this manner allows the strength reserve of postbuckling composite design to be exploited, which has application for the next generation of composite aerospace structures.

REFERENCES

[1] R. Zimmermann, H. Klein and A. Kling, Buckling and postbuckling of stringer stiffened fibre composite curved panels − tests and computations. *Composite Structures*, **73**, 150-161, 2006.

[2] R. Degenhardt, R. Rolfes, R. Zimmerman and K. Rohwer, COCOMAT – Improved MATerial Exploitation at Safe Design of COmposite Airframe Structures by Accurate Simulation of COllapse. *Composite Structures*, **73**, 178-178, 2006.

[3] COCOMAT Home Page, www.cocomat.de, 2007.

[4] A. C. Orifici, *Degradation Models for the Collapse Analysis of Composite Aerospace Structures*. PhD thesis, Royal Melbourne Institute of Technology, 2007.

[5] L. Tong, An assessment of failure criteria to predict the strength of adhesively bonded double lap joints. *Journal of Reinforced Plastics and Composites*, **16**, 698-715, 1997.

[6] A. C. Orifici, I. Herszberg, R. S. Thomson, T. Weller, A. Kotler, and J. Bayandor, Failure in stringer interfaces in postbuckled composite stiffened panels. *12th Australian International Aerospace Congress*, Melbourne, Australia, 19-22 March, 2007.

[7] Z. Hashin, Failure criteria for unidirectional composites. *Journal of Applied Mechanics*, **47**, 329-334, 1980.

[8] F. K. Chang and L. B. Lessard, Damage tolerance of laminated composites containing an open hole and subject to compressive loadings: part I − analysis. *Journal of Composite Materials*, **25**, 2-43, 1991.

[9] A. C. Orifici, R. S. Thomson, R. Degenhardt, C. Bisagni and J. Bayandor, Development of a finite element methodology for the propagation of delaminations in composite structures. *Mechanics of Composite Materials*, **43**, 1, pp. 9-28, 2007.

[10] A. C. Orifici, R. S. Thomson, R. Degenhardt, S. Büsing and J. Bayandor, Development of a finite element methodology for modelling mixed-mode delamination growth in composite structures. *12th Australian International Aerospace Congress*, Melbourne, Australia, 19-22 March, 2007.

[11] E. F. Rybicki and M. F. Kanninen, A finite element calculation of stress intensity factors by a modified crack closure integral. *Engineering Fracture Mechanics*, **9**, 931-938, 1977.

[12] R. Krueger, *The Virtual Crack Closure Technique: History, Approach and Applications*, NASA/CR-2002-211628, ICASE Virginia, USA, 2002.

[13] M. L. Benzeggagh and M. Kenane, Measurement of mixed-mode delamination fracture toughness of unidirectional glass/epoxy composites with mixed-mode bending apparatus. *Composites Science and Technology*, **56**, 439-449, 1996.

[14] P. P. Camanho and C. G. Dávila, *Mixed-Mode Decohesion Finite Elements for the Simulation of Delamination in Composite Materials*, NASA/TM-2002-211737, NASA Langley Research Center, Virginia, USA, 2002.

[15] R. Degenhardt, A. Kling, H. Klein, W. Hillger, H. C. Goetting, R. Zimmermann, K. Rohwer and A. Gleiter, Experiments on buckling and postbuckling of thin-walled CFRP structures using advanced measurement systems. *International Journal of Structural Stability and Dynamics*, **7**, 2, 337-358, 2007.